


# Vibrational motion of a vortex lattice induced near the surface of a type-II superconductor by an external low-frequency ac magnetic field

K. S. Pigalskiy *N.N. Semenov Federal Research Center for Chemical Physics, Russian Academy of Sciences, ul. Kosygina 4, Moscow 119991, Russia*

(Received 1 October 2020; revised 6 January 2021; accepted 8 February 2021; published 22 February 2021)

The theoretical description and experimental study of a reversible vibrational vortex motion induced in a type-II superconductor by a weak low-frequency ac magnetic field are discussed. The case where the external magnetic field and vortex lines are parallel to the surface of the superconductor is considered. The equilibrium positions of vortices near a surface, the amplitude of their vibrations, and the contribution of this process to the dynamic permeability  $\mu_v$  are calculated. In these calculations, the interactions of vortices with each other, with the surface, and with pinning centers are considered within the discrete vortex lattice model. The calculations in the London approximation are compared with the results obtained within a more accurate model, including the spatial variation of the order parameter in the vortex core by means of a variational function. It is shown that the structural parameters of the vortex lattice near the surface depend on the accuracy of the description of the intervortex interactions, but the contribution  $\mu_v$  appears to be model independent. It is important that this conclusion is valid in the case of the exponential approximation for the interaction between vortex rows. In this approximation, the problem under consideration is analytically examined, and formulas describing the dependences of the parameters of the vortex lattice and the contribution  $\mu_v$  on the external dc magnetic field and the characteristics of a superconductor are derived. The theoretical results are compared with experimental data for a  $\text{YBa}_2\text{Cu}_3\text{O}_y$  high- $T_c$  superconducting single-crystal plate. The magnetic field is parallel to the plate, i.e., to the crystallographic  $ab$  plane. A strong anisotropy of the properties and shape of the crystal is considered when analyzing the experimental data. A procedure for the determination of the experimental dependence  $\mu_v(H)$  is described. It is shown that the reversible vibrations of vortices occur near the planes of the single-crystal plate in the direction of the crystallographic  $c$  axis, whereas vortices enter its lateral ends and leave them (along the structural layers) even at a small magnetic field amplitude of about 1 Oe. It is found that the developed theoretical description reproduces the experimental data  $\mu_v(H)$  in the entire studied range of temperatures and magnetic fields under the assumptions that pinning is isotropic and the length of interaction of vortices with pinning centers is close to the coherence length.

DOI: [10.1103/PhysRevB.103.064509](https://doi.org/10.1103/PhysRevB.103.064509)

## I. INTRODUCTION

Experimental methods based on the measurements of quantities characterizing the response of a type-II superconductor to an external ac magnetic field are widely used to obtain information on the properties of a vortex system. Various regimes of motion of vortices can be induced, depending both on the amplitude  $H_m$  and frequency  $\omega$  of the ac magnetic field and on the parameters of the vortex system (the density of vortices, the degree of their anisotropy, and the relation between the magnitudes of interactions of vortices with each other, with the surface, and with pinning centers).

The vibrations of vortices near equilibrium positions are of fundamental and applied significance. This regime was first revealed and studied by Campbell [1,2], who proposed a phenomenological description of the response of a sample to a weak low-frequency ac field based on the consideration of the reversible vibrations of vortices in a potential well produced by the interaction of a vortex with pinning centers.

Owing to this process, the ac field penetrates the sample to the effective depth  $\lambda_C$  called the Campbell penetration depth. The  $\lambda_C$  value is determined primarily by the slope of the pinning well, which is characterized by the Labusch constant  $\alpha_L$ .

The theory of this phenomenon was significantly developed after the discovery of high- $T_c$  superconductors (HTSCs). Brandt [3,4], Coffey and Clem [5], Clem and Coffey [6], and other authors [7–9] additionally considered the elasticity of the vortex lattice, viscous friction, proximity to the surface, and other factors. The calculations in the cited papers, as well as in Refs. [1,2], were performed in the continuum approximation for the local vortex density. It is noteworthy that many corrections obtained for the Campbell formula become insignificant in the low-frequency limit, and the expression for the square of the penetration depth of the ac magnetic field is reduced to the form

$$\lambda_{ac}^2 = \lambda^2 + \lambda_C^2 = \lambda^2 + \frac{B^2}{4\pi\alpha_L}. \quad (1)$$

Here,  $\lambda$  is the London penetration depth, and  $B$  is the magnetic induction near the surface.

\*pigalskiy@gmail.com

Experimental studies of HTSCs in the ac magnetic field showed that the vibrations of vortices strongly affect the magnetic characteristics. Measurements of the permeability at the fundamental and third harmonics for  $\text{YBa}_2\text{Cu}_3\text{O}_y$  (YBaCuO) powder samples carried out in Ref. [10] revealed that the contribution of reversible motion increases with the dc field and temperature. Using the Campbell model, the authors of Refs. [11,12] determined the parameters of the pinning well near the irreversibility line. In particular, the temperature dependences of the critical current density  $J_c$ , the Labusch constant, and the length of interaction of the vortex with pinning centers were determined in Ref. [11] for YBaCuO melt-textured ceramic. The measurements performed in the linear (Campbell) and nonlinear (dissipative) regimes of vortex motion provided information on the nature of the peak effect (anomalous increase in  $J_c$  in the considered regions of fields and temperatures). In Ref. [13], the Campbell method was used to analyze the effect of  $\text{BaZrO}_3$  nanoparticles on pinning in a YBaCuO nanocomposite film. It was shown that the introduction of impurity nanoparticles results in an anomalous increase in the Labusch constant  $\alpha_L(H,T)$  with an increase in the dc magnetic field at all temperatures. Considering the reversible vortex motion, the authors of Ref. [14] determined the critical current density  $J_c$  in the film from the measurement of nonlinear properties at the third harmonic. The critical current density  $J_c$  thus determined appeared to be overestimated; this overestimate is larger for a thinner film. The overestimate factor is about  $\lambda_C/D$  ( $D$  is the thickness of the film).

The hysteresis of the Campbell penetration depth detected in Ref. [15] for HTSCs with a high degree of anisotropy (e.g., in Bi-based superconductors) is of interest. It was found that the depth  $\lambda_C$  depends on the prehistory of the formation of the vortex system: in the first case, the sample was cooled in a magnetic field (FC mode), whereas in the second case, the field was applied after cooling in zero field (ZFC mode). A smaller  $\lambda_C$  value in the FC mode compared with the ZFC mode was attributed by the authors to the difference in the curvature of the pinning potential well (i.e.,  $\alpha_L$  values) near its bottom or near the edge because the gradient of the magnetic field in the ZFC mode is much larger, and vortices are located closer to the edge of the well. The discovery of this effect stimulated a cycle of theoretical papers [16–18], where a quantitative relation between the Campbell penetration depth and the microscopic parameters of the pinning energy landscape was established within strong pinning theory.

The Campbell model implies the existence of quite strong pinning, at which the size of the pinning potential well is smaller than the intervortex distance. In the case of weak pinning (e.g., near the irreversibility line),  $\alpha_L \rightarrow 0$ , and Eq. (1) is inapplicable because the positions of vortices become unstable and  $\lambda_{ac}$  tends to infinity in the low-frequency limit.

In the regime of reversible vortex vibrations, the variable component of the magnetic field should displace vortices near the equilibrium positions, i.e., the amplitude  $H_m$  should not exceed the external field interval  $\Delta H_{vs}$ , where a vortex lattice is only elastically deformed, whereas the number of vortices in the sample does not change. In the considered strong pinning models, the interval  $\Delta H_{vs}$  corresponds to the displacement of vortices from one edge of the potential well

to the opposite edge, which is accompanied by change of the sign of the pinning force.

However, the vibrational regime of vortex motion can also occur in the absence of pinning if a finite interval  $\Delta H_{vs}$  of another nature exists. One of such mechanisms is well known and is due to the surface energy barrier for the entry and exit of vortices (the Bean-Livingston surface barrier [19]). It is noteworthy that the barrier for the entry of vortices (determined by the condition for the nucleation of a vortex near the surface of the superconductor) and the barrier for exit (caused by the electromagnetic interaction of the vortex with the surface) have different physical natures and, as a result, different field dependences. In particular, the barrier for the entry of vortices through a flat superconductor-insulator interface vanishes in a field of  $H > H_c$ , whereas the barrier for the exit of vortices remains finite up to fields  $H \sim H_{c2}$  [20] (where  $H_c$  and  $H_{c2}$  are the thermodynamic and upper critical fields, respectively).

The continuum approximation is often insufficient to calculate the characteristics of the vortex system near the surface, and it is necessary to use the discrete vortex lattice model. Vibrations of vortices for the case of negligibly weak pinning were theoretically considered in Refs. [21–25] within the discrete model. The calculations were performed in the London approximation (LA), and an expression was obtained for the contribution  $\mu_v$  of this process to the dynamic permeability of a plate sample in a magnetic field parallel to the plate. It was shown that the calculations reproduce the experimental data for the YBaCuO single crystal in a temperature range from 70 K to  $T_c$  and in a weak dc field. The discrete vortex lattice model was also used in Ref. [26] to calculate elastic constants at the shift of vortices along and across the system of planar pinning centers.

The vibrational contribution to the permeability was calculated in Ref. [27] within the discrete model more accurately than in the LA. The decrease in the order parameter in the vortex core was considered by the variational function proposed in Refs. [28,29]:

$$f(\rho) = \frac{f_\infty \rho}{(\rho^2 + \xi_v^2)^{1/2}}. \quad (2)$$

Here,  $\rho$  is the distance from the center of the vortex and  $\xi_v$  and  $f_\infty$  are the effective radius of the core and the order parameter far from the center of the vortex, respectively, which are variational parameters determined from the condition of the thermodynamic potential minimum. For an isolated vortex,  $\xi_v = \sqrt{2}/\kappa$  and  $f_\infty = 1$  (at Ginzburg-Landau parameter  $\kappa \gg 1$ ).

The variational method (VM) makes it possible to more accurately calculate the field of the vortex compared with the LA and, consequently, the intervortex interactions, as well as to consider a change in the self-energy of the vortex in fields  $H \gg H_{c1}$ , in which the overlap of vortex cores begins to be noticeable (here,  $H_{c1}$  is the lower critical field). This method allows a sufficiently accurate calculation of the equilibrium magnetization in the entire magnetic field range  $H_{c1} \leq H \leq H_{c2}$  [29–31]. The VM was also applied in Ref. [27] to calculate the magnetodynamic response of the vortex lattice. However, only a particular case of an ideal triangular lattice

neglecting its distortions near the surface was considered in Ref. [27], and the effect of pinning on  $\mu_v$  was not analyzed.

In this paper, problems of the theoretical description and experimental study of the properties of a vortex lattice undergoing reversible vibrations under the action of an external low-frequency ac magnetic field are consistently analyzed. Numerical calculations are performed in Sec. II, where the structure of the vortex lattice near the surface and the corresponding vibrational vortex contribution  $\mu_v$  to the dynamic permeability are also analytically described. The basic relations determining the static and low-frequency dynamic properties of the vortex system within the discrete model are presented. Further, in the weak pinning approximation, the dependence of the results of calculations on the accuracy of the approximation used to describe intervortex interactions is comparatively analyzed. Finally, methods for the inclusion of pinning, its effect on the magnetodynamic properties of the vortex lattice, and problems of numerical calculations are considered in Sec. II, where a method for the analytical description of the vortex system with pinning is also proposed. An experimental approach to obtain quantitative information on  $\mu_v$  and the critical current for a YBaCuO HTSC single-crystal plate in a magnetic field parallel to the surface is described in Sec. III. Experimental field dependences  $\mu_v(H)$  are analyzed in Sec. IV within the developed theoretical concepts. Finally, the conclusions are formulated in Sec. V.

## II. THEORY

### A. Basic relations

The properties of the vortex system are calculated within the commonly accepted discrete vortex lattice model near the flat boundary of the superconductor when vortex lines are parallel to the boundary. In this model, the vortex lattice is nearly triangular and consists of rows parallel to the surface. The distance between vortices along all rows is the same and denoted as  $a$ . The positions of vortices in neighboring rows are shifted by  $a/2$ . A magnetic field is directed along the  $z$  axis, which is parallel to the surface; the  $x$  axis is perpendicular to the surface; and the  $y$  axis is directed along the rows. This geometry is quite appropriate to a superconducting plate sample when the external field is parallel to its larger face. For simplicity, we consider an isotropic case and the anisotropy of a real HTSC crystal is taken into account when discussing experimental data.

The equilibrium position  $x_n$  of the  $n$  th row is determined by the balance condition for all forces acting on each vortex in this row:

$$F_M(x_n) + \sum_{i=1}^{n-1} F_v(x_n - x_i) - \sum_{i=n+1}^{\infty} F_v(x_i - x_n) - \sum_{i=1}^{\infty} F_v(x_i + x_n) + F_p = 0. \quad (3)$$

Here, the first term is the force induced by the Meissner screening current; the second and third terms are the forces induced by other rows of vortices located nearer and farther from the surface than the  $n$  th row, respectively; the fourth term is the attraction force to the system of images; and the

fifth term is the pinning force (which is negative and positive for increasing and decreasing external dc fields, respectively). In the considered geometry, the effects associated with a finite size of the superconductor  $L$  along the  $z$  axis and with the intersection of its boundary by vortex lines are neglected. These effects are significant if  $L$  is not larger than  $\lambda$  [32]. The system of Eq. (3) allows the calculation of the structure of the vortex lattice and, thereby, its physical properties.

In this paper, the complex permeability is an experimentally measured quantity characterizing the penetration of the ac magnetic field into the sample. The real part  $\mu'$  of the permeability in the external magnetic field  $H(t) = H + H_m \sin(\omega t)$  is defined as

$$\mu'(H) = \frac{1}{2\pi H_m} \int_0^{2\pi/\omega} \cos(\omega t) \left[ \frac{dB(H, t)}{dt} \right] dt. \quad (4)$$

Contributions to  $\mu'$  of various physical origins were considered in Refs. [21,23]. In the limit of small amplitude, where the number of vortices in the sample remains constant, the time-dependent part of the magnetic induction contains two components:  $B(H, t) = B_M(t) + B_v(H, t)$ . The first component is related to the oscillation of the Meissner screening current, and the second component is due to the vibrations of vortices near the equilibrium positions. These processes make two contributions to the permeability:  $\mu' = \mu_M + \mu_v$ . The Meissner contribution is independent of the external field; for a plate sample with the thickness  $D \gg \lambda$ , considering the penetration of the field from both sides of the plate, it is

$$\mu_M = \frac{2\lambda}{D}. \quad (5)$$

In the case of vibrational motion, when the number of vortices in the sample does not change, the discrete model makes it possible to refine the physical nature of the variation of the magnetic induction. As known, the magnetic flux of the vortex  $\Phi$  near the boundary of the superconductor is smaller than the magnetic flux quantum  $\Phi_0$  and depends on the distance  $x$  between the vortex and the surface. For the flat boundary,  $\Phi = \Phi_0[1 - \exp(-x/\lambda)]$ . As a result, both the amplitude of the time variation of  $B_v$  and the vibrational contribution to the permeability  $\mu_v$  are determined by the characteristics of motion of vortices located in a relatively thin near-surface layer with a thickness of  $\sim \lambda$ . This circumstance allowed the theoretical consideration in Ref. [23], where the following expression was obtained for the vibrational contribution to the permeability:

$$\mu_v = \frac{2\Phi_0}{Da\lambda} \sum_n \exp\left(-\frac{x_n}{\lambda}\right) \left(\frac{\delta x_n}{\delta H}\right). \quad (6)$$

The formula in Eq. (6) allows the calculation of  $\mu_v$  in terms of the positions of vortex rows  $x_n$  and their shifts  $\delta x_n$  under a small variation of the external field  $\delta H$ .

Expressions for intervortex interaction forces entering Eq. (3) depend on the used model. The calculations were carried out within three models: the LA, the VM considering the structure of the core, and the exponential approximation (EA), which is a simplified variant of the LA, where the force with which a vortex row acts on a probe vortex is described by an exponential function.

Below, we use the dimensionless Ginzburg-Landau units, where the length is measured in units of  $\lambda$ , and the magnetic field is measured in units of  $\sqrt{2}H_c$ . In these units,  $\Phi_0 = 2\pi/\kappa$ ,  $H_{c2} = \kappa$ , and the force is measured in units of  $\kappa\Phi_0^2/8\pi^2\lambda^3$ . The dimensionless magnetic field, magnetic induction, and force will be denoted by lowercase letters to distinguish them from the respective dimensional physical quantities.

The expression for the force with which the Meissner current acts on the vortex is model independent and has the form

$$f_M(x) = h \exp(-x). \quad (7)$$

As known, the field generated by a vortex at the distance  $\rho$  from its center in the LA has the form

$$b_0^{\text{LA}}(\rho) = \frac{1}{\kappa} K_0(\rho), \quad (8)$$

where  $K_0$  is the modified Bessel function of the second kind. The total field generated by a row of vortices at the distance  $x$  was calculated in Ref. [33]. The gradient of this field gives the force with which the row of vortices acts on the probe vortex in another row:

$$f_v^{\text{LA}}(x) = \frac{\pi}{\kappa a} \left[ \exp(-x) \mp 2 \frac{\exp(-2\pi x/a)}{1 \pm \exp(-2\pi x/a)} \right]. \quad (9)$$

Here, the upper and lower signs correspond to the positions of the probe vortex with the shift by  $a/2$  along the  $y$  axis with respect to the positions of vortices in the row and without such shift, respectively.

Within the VM, when the spatial variation of the order parameter in the vortex core is described by the function in Eq. (2), the expression for the field of an isolated vortex was calculated in Ref. [29]:

$$b_0^{\text{VM}}(\rho) = \frac{f_\infty}{\kappa \xi_v K_1(f_\infty \xi_v)} K_0\left(f_\infty \sqrt{\rho^2 + \xi_v^2}\right). \quad (10)$$

Fields given by Eq. (10) were summed for the row of vortices in Ref. [30], and the corresponding force acting on the probe vortex within the VM is given by the expression

$$f_v^{\text{VM}}(x) = \frac{\pi f_\infty}{\kappa a \xi_v K_1(f_\infty \xi_v)} \frac{x}{x_c} \times \left[ \exp(-f_\infty x_c) \mp 2 \frac{\exp(-2\pi x_c/a)}{1 \pm \exp(-2\pi x_c/a)} \right], \quad (11)$$

where  $x_c = (x^2 + \xi_v^2)^{1/2}$ .

We consider the practically significant field range  $H < 0.5H_{c2}$ , where the overlap of the vortex cores can be neglected and  $f_\infty = 1$  can be set [29]. Figure 1 shows the force with which the row of vortices acts on the probe vortex calculated within various models as a function of the distance between the row and the probe vortex. The distance between the vortices along the row corresponds to the field  $h = 20$ , and the parameter  $\xi_v = \xi_{v0} = \sqrt{2}/\kappa$  corresponds to the isolated vortex [29]. Arrows mark the distances to the three nearest rows; the distance between neighboring rows is  $d = \sqrt{3}a/2$ . As seen, differences associated with the decrease in the order parameter in the vortex core are manifested only for several nearest rows. The inclusion of the core most strongly reduces the repulsion force between vortices in the neighboring rows.

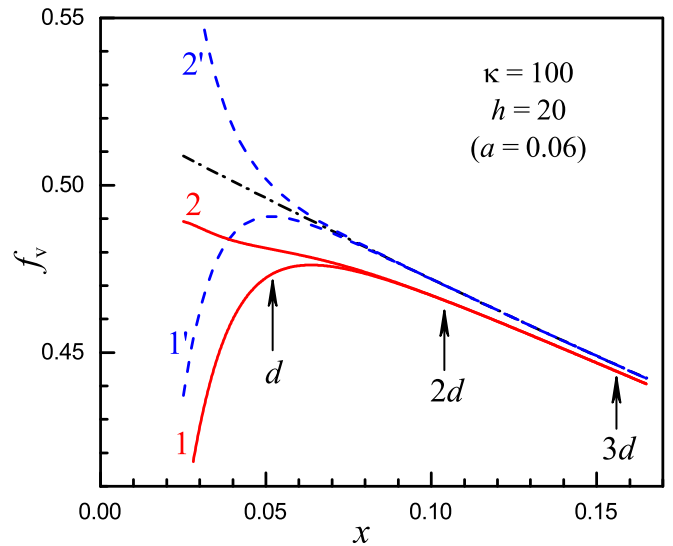


FIG. 1. Force with which the row of vortices acts on the probe vortex vs the distance to it as calculated (solid lines) by the variational method (VM), (dashed lines) in the London approximation (LA), and (dash-dotted line) in the exponential approximation (EA) in the case of (1,1') the shift of the probe vortex with respect to the positions of vortices in the row by  $a/2$  and (2,2') without shift. Arrows mark the distances to the three nearest rows.

The dash-dotted line is the distance dependence of the force calculated within the EA:

$$f_v^{\text{EA}}(x) = \frac{\pi}{\kappa a} \exp(-x). \quad (12)$$

The expression in Eq. (12) is obtained from Eq. (9), where the correction considering the mutual arrangement of vortices along the  $y$  axis (the second term in the square brackets) is omitted. It is seen that this simplification is manifested only in the interaction between the neighboring rows. This approximation is important for the consideration of the structure and dynamics of the vortex lattice near the surface because it allows the analytical solution of the problem with pinning.

We now consider how the accuracy of the description of intervortex interaction forces affects the position and mobility of vortex rows and, as a result, the vibrational permeability  $\mu_v$  for the case of negligibly weak pinning.

## B. Case of negligibly weak pinning

In the limit of weak pinning ( $F_p = 0$ ), the gradient of the density of vortices in the bulk of the superconductor is absent, the vortex lattice is triangular and is in a state close to the thermodynamic equilibrium with the external field. A small positive or negative deviation of the magnetic induction  $b_v$  inside the superconductor from the equilibrium value  $b_{\text{eq}}$  can occur due to the surface barrier. The corresponding hysteretic behavior of  $b_v$  upon the increase and decrease in the magnetic field was discussed in Refs. [24,25,34]. Below, we neglect this effect and consider only the equilibrium state  $b_v = b_{\text{eq}}$ . This state corresponds to the minimum of the Gibbs free energy,

which for the triangular lattice is given by the expression [35]

$$G = \frac{\kappa b_v}{2\pi} \left[ \varepsilon_0 + \frac{12\pi}{\kappa} \sum_{n=1}^{\infty} \sum_{m=0}^{\infty} b_0(a\sqrt{n^2 + nm + m^2}) \right] - 2b_v h. \quad (13)$$

Here,  $\varepsilon_0$  is the self-energy of the vortex per unit length, and  $b_0(\rho)$  is the field of the vortex; expressions for these quantities are different in different approximations. In the LA,  $b_0(\rho)$  is given by Eq. (8), and  $\varepsilon_0$  is specified as (see, e.g., Ref. [36])

$$\varepsilon_0^{\text{LA}} = \frac{2\pi}{\kappa^2} [\ln(\kappa) + C_1]. \quad (14)$$

The constant  $C_1$  cannot be determined in the LA; its value  $C_1 = 0.4968$  was calculated in Ref. [37]. In the variational model,  $b_0(\rho)$  has the form of Eq. (10), and the expression for  $\varepsilon_0$  was obtained in [29]

$$\varepsilon_0^{\text{VM}} = \frac{\pi \xi_v^2}{2} + \frac{\pi}{2\kappa^2} + \frac{2\pi K_0(\xi_v)}{\kappa^2 \xi_v K_1(\xi_v)}. \quad (15)$$

The minimization of the Gibbs free energy allows determination of the equilibrium magnetic induction  $b_{\text{eq}}$  and the corresponding distance between the vortices along the rows  $a_{\text{eq}} = (4\pi/\sqrt{3}\kappa b_{\text{eq}})^{1/2}$ , as well as the variational parameter  $\xi_v$  in the VM.

In the considered thermodynamically equilibrium state, the vortex structure and its properties are single-valued functions of  $h$ . Calculations included several stages. Considering possible distortions of the vortex lattice near the surface, the equilibrium positions  $x_n$  of  $N_r$  vortex rows nearest to the surface, which satisfy the force balance conditions in Eq. (3), were determined in the first stage by means of a numerical procedure. Distortions of the regular triangular lattice for more remote rows, beginning with  $N_r + 1$ , were neglected, and the distance between rows was assumed to be  $d_{\text{eq}} = \sqrt{3}a_{\text{eq}}/2$ . In the second stage, a small variation of the external field  $\delta h$  was introduced with the conservation of  $b_v$ . After that, the shifts  $\delta x_n$  of the equilibrium positions of the vortex rows were determined, which allowed calculating the parameters  $C_n = (\delta x_n / \delta h)$  characterizing the mobility of the vortex lattice. In the last stage, the vibrational permeability  $\mu_v$  was determined by Eq. (6). The calculations for large values  $N_r > 5$  required the development of a special slow descent algorithm to approach the equilibrium  $x_n$  values because the simple successive search for equilibrium positions, beginning with the first row, led to an unstable solution.

Figures 2, 3, and 4(a) show the field dependences of the distance to the first row  $x_1$ , its mobility  $C_1$ , and the resulting vibrational permeability  $\mu_v$  calculated within various models and at various  $N_r$  values (the Ginzburg-Landau parameter  $\kappa = 100$ ). We first consider the case  $N_r = 1$ , where possible distortions of the triangular vortex lattice near the surface are neglected. It is seen that the  $x_1(h)$ ,  $C_1(h)$ , and  $\mu_v(h)$  curves obtained within different models are significantly different. This conclusion for the case of  $N_r = 1$  was also made in Ref. [27]. The  $x_1$  value obtained in the LA decreases monotonically with increasing field, whereas the  $x_1(h)$  dependence obtained within the VM is nonmonotonic, and the first row is anomalously shifted from the surface in high fields. Furthermore, the mobility of the first row  $C_1$  obtained within the VM is noticeably lower than that in the LA. Consequently, the

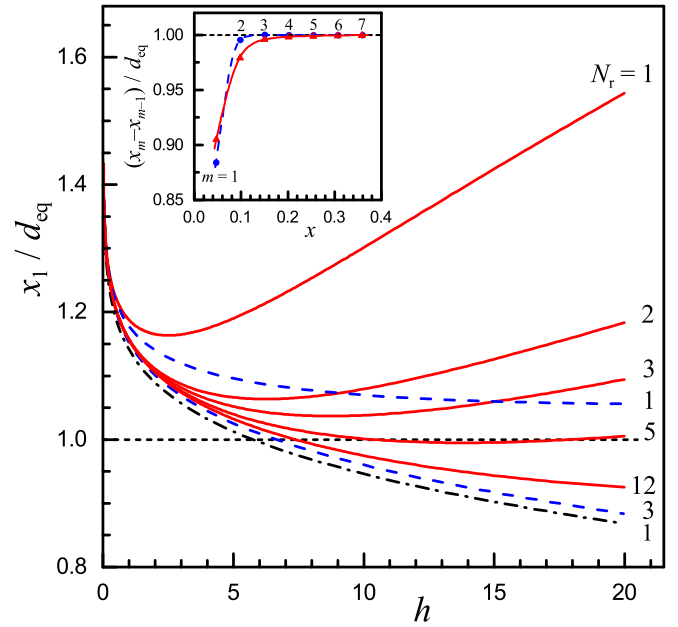


FIG. 2. Field dependences of the distance from the surface to the first vortex row calculated (solid lines) by the variational method (VM), (dashed lines) in the London approximation (LA), and (dash-dotted line) in the exponential approximation (EA). The numbers of rows whose positions were determined from the force balance conditions in Eq. (3) are indicated next to the lines. The inset shows the normalized distances from the surface to the first vortex row and between rows vs the position of the row ( $h = 20$ ,  $N_r = 24$ ).

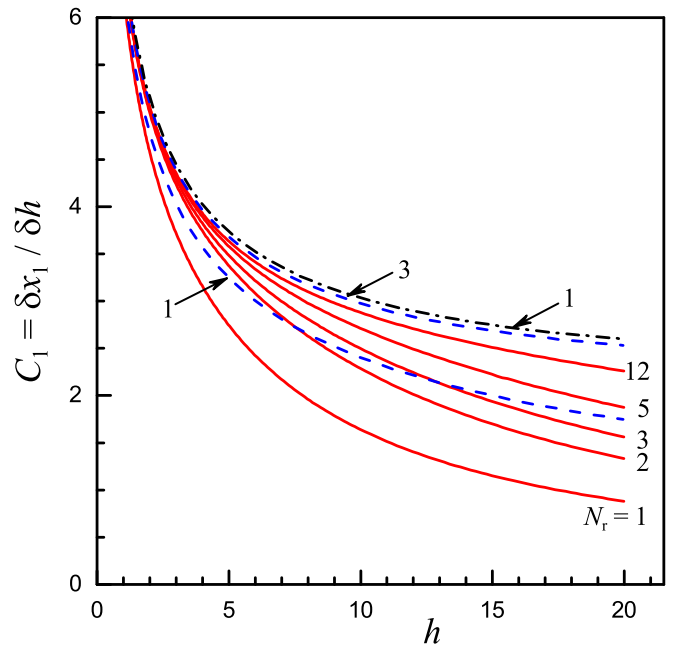


FIG. 3. Field dependences of the shift of the first row of vortices under a small variation of the external field calculated (solid lines) by the variational method (VM), (dashed lines) in the London approximation (LA), and (dash-dotted line) in the exponential approximation (EA). The numbers of near-surface rows whose positions were determined from the force balance conditions are indicated next to the lines.

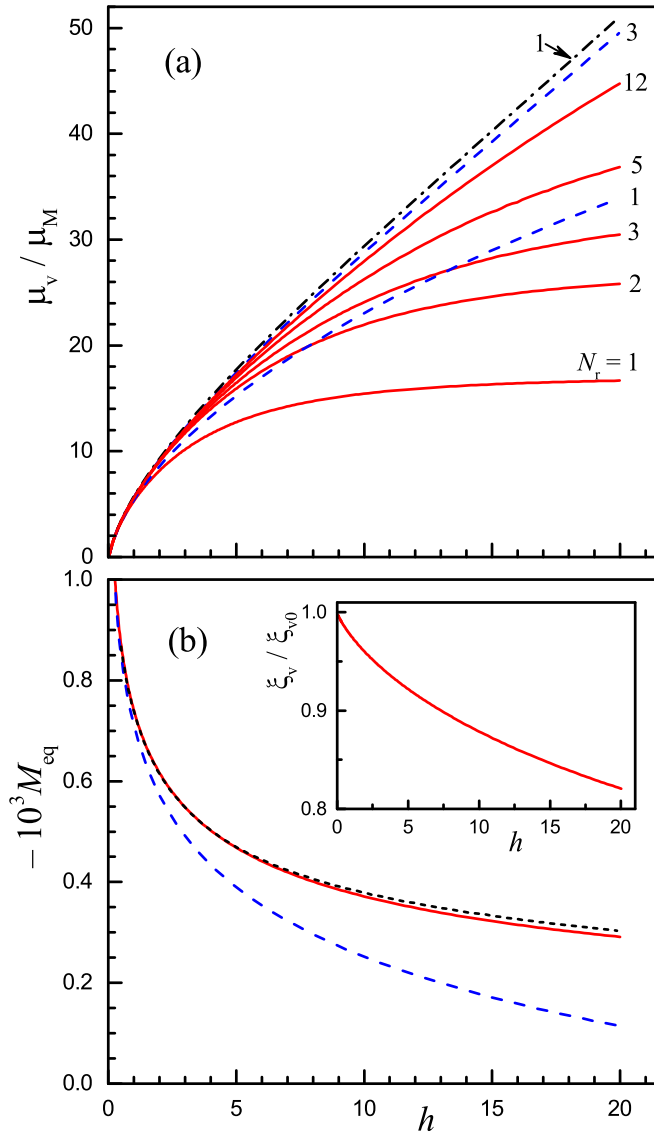


FIG. 4. (a) Field dependences of the contribution from the vibrations of vortices to the permeability calculated (solid lines) by the variational method (VM), (dashed lines) in the London approximation (LA), and (dash-dotted line) in the exponential approximation (EA). The numbers of rows whose positions were exactly determined from the force balance condition are indicated next to the lines. (b) Field dependences of the equilibrium magnetization calculated (solid line) by the VM, (long dashed line) in the LA, and (short dashed line) by the analytical formula taken from Ref. [31]. The inset shows the field dependence of the variational parameter  $\xi_v$ .

dependences  $\mu_v(h)$  also differ [see Fig. 4(a)]. The vibrational permeability  $\mu_v$  obtained within the VM is smaller than that in the LA and is saturated in high fields.

Calculations with larger  $N_r$  values carried out in this paper give a surprising result. With an increase in the number of rows  $N_r$ , whose positions were exactly determined from the force balance equations, the dependence  $\mu_v(h)$  becomes model independent [see Fig. 4(a)]. At the same time, some differences in the  $x_1(h)$  and  $C_1(h)$  curves hold. It is important that the same dependence  $\mu_v(h)$  was obtained in the simplest

EA; the result evaluated in this approximation is shown by the dash-dotted line in Fig. 4(a).

A strong dependence of the results obtained within the VM on  $N_r$  indicates that the core-induced distortions of the triangular lattice near the surface are larger than those in the LA. This difference is demonstrated in the inset of Fig. 2, where the distances from the first row to the surface ( $m = 1$ ) and between rows ( $m > 1$ ) calculated in the LA and VM (at  $N_r = 24$ ) are shown. It is seen that the concentration of rows near the surface within the VM is higher, but the first row is farther from the surface. These two factors apparently compensate each other, and this compensation is one of the reasons for the constancy of the resulting  $\mu_v$  value.

The model independence of the calculated vibrational contribution to the permeability is a quite unique property. Calculations within these models give strongly different field dependences of the equilibrium magnetization [see Fig. 4(b)]. The LA is applicable only in a narrow field range near  $H \sim H_{c1}$ . Reasons for the strong effect of the structure of the vortex core on the magnetization at  $H \gg H_{c1}$  were discussed in detail in Refs. [29–31,38], where methods for the calculation of the variational parameters and the magnetization are also presented.

The positions of vortex rows calculated in the EA are independent of  $N_r$ , and the triangular lattice is not distorted near the surface. This result was previously obtained analytically in Ref. [20] and numerically in Ref. [23]. It is likely due to the identical exponential form of the interactions of rows with each other and with the external field. It is important that this approximation makes it possible to derive analytical expressions for the considered quantities. Corresponding calculations for the case of negligibly weak pinning were carried out in Refs. [24,25]. The position of the first row is given by the expression

$$x_1 = \frac{d_{\text{eq}}}{2} + \ln \left[ \frac{h}{\tilde{b}_v} + \sqrt{\left(\frac{h}{\tilde{b}_v}\right)^2 - 1} \right], \quad (16)$$

where

$$\tilde{b}_v = b_v \frac{d_{\text{eq}}}{2 \sinh(d_{\text{eq}}/2)}. \quad (17)$$

The shift of the first row of vortices under a small variation of the external field is

$$\delta x_1 = \frac{\delta h}{\sqrt{h^2 - \tilde{b}_v^2}}. \quad (18)$$

The contribution to the permeability from the vibrations of the vortex lattice has the form

$$\mu_v = \mu_M \frac{2\alpha_1^2}{\alpha_0 - \alpha_1^2}, \quad (19)$$

where

$$\alpha_1 = \exp(-x_1), \quad \alpha_0 = \exp(-d_{\text{eq}}). \quad (20)$$

In Figs. 2, 3, and 4(a), analytical dependences calculated by Eqs. (16)–(20) coincide with the numerical results obtained

in the EA (dash-dotted lines). Furthermore, the function in Eq. (19) describes the common asymptote of the  $\mu_v(h)$  curves calculated in different models with increasing  $N_r$ .

### C. Effect of pinning

The interaction of the vortex lattice with pinning centers affects both the equilibrium positions of vortex rows and the amplitude of their vibrations. As known, the pinning force depends on the position of the vortex inside the potential well and reaches the maximum  $p$  near its edge. If the gradient of the magnetic induction changes sign, the pinning force can vary in the range  $-p \leq f_p \leq p$ . The maximum pinning force  $p$  (per unit length of the vortex) is related to the critical current density  $J_c$  (in units of A/cm<sup>2</sup>) as

$$p = \frac{4\pi^2\lambda^3}{5\kappa\Phi_0} J_c. \quad (21)$$

To calculate  $x_n(p)$ , we include pinning forces in the force balance conditions in Eq. (3). Following the above sequence of calculations, we first numerically determine the positions of  $N_r$  rows near the surface by solving the system of Eq. (3) under the assumption that the rows  $n > N_r$  satisfy the condition  $(x_{n+1} - x_n) = (x_{N_r} - x_{N_r-1})$ . Uncertainty associated with the existence of an infinite set of possible solutions appears already in this stage of calculations. The reason is that the additional condition of the existence of the thermodynamically equilibrium vortex lattice at  $x \gg \lambda$  in the case of unpinned vortices is inapplicable in the presence of pinning. Therefore, to obtain an unambiguous solution in the case of pinning, it is necessary to introduce a new physically justified criterion.

The first obvious requirement to this criterion is the continuous passage to the results for the unpinned lattice in the limit  $p \rightarrow 0$ . We also assume that the vortex system near the surface most closely approaches the thermodynamic equilibrium with the external field. This postulate was used in numerous papers, for example, when calculating the magnetization of a hard superconductor, which were in good agreement with experiment (see, e.g., Refs. [39,40]). The additional condition in the EA in the form

$$(x_2 - x_1) = d_{\text{eq}}, \quad (22)$$

satisfies both requirements. In particular, the first requirement is satisfied because of the absence of distortions of the triangular lattice at  $p = 0$  in the EA, for which the distance between all rows, including two rows nearest to the surface, is  $d_{\text{eq}}$ . Thus, without loss of generality, the EA with the condition given by Eq. (22) is used in the further numerical calculations and in the derivation of analytical expressions.

The dependence of changes in the positions of vortex rows near the surface calculated on the pinning force is shown in Fig. 5 for the case of increasing external field, where the pinning force prevents the penetration of vortices, and the vortex rows nearest to the surface are shifted toward it. Figure 5 also demonstrates the opposite effect of pinning. The appearing gradient of the magnetic induction, which is caused by a decrease in the density of vortices with an increase in the distance from the surface, is responsible for the shift of vortex rows deeper inside the superconductor beginning with a certain row.

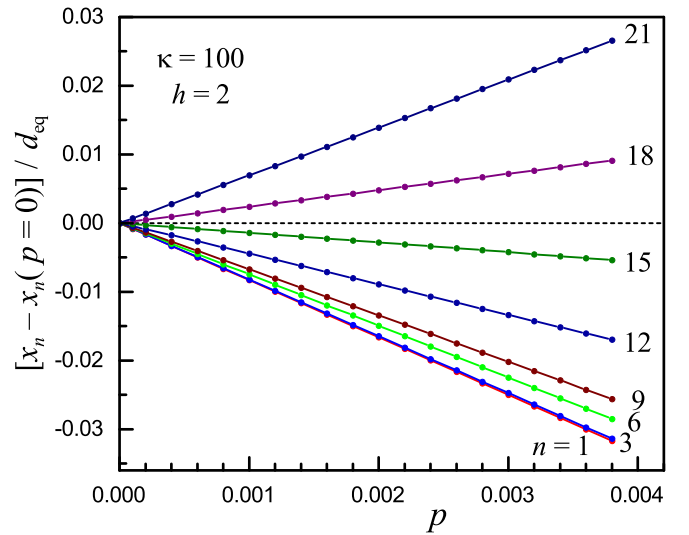


FIG. 5. Shift of vortex rows vs the pinning force directed to the surface (the case of an increase in the external magnetic field). The row numbers are indicated next to the lines.

The next step in the calculations was the determination of the shift  $\delta x_n$  of vortex rows under a small variation of the external field  $\delta h$ . Since this shift occurs inside the pinning potential well, it is necessary to include the appearing returning force  $\delta f_p = -k_p \delta x_n$  in the force balance conditions in Eq. (3). (This problem is discussed in more detail in Appendix B). The corresponding force constant  $k_p$  characterizing the slope of the well at the vortex center position is related to the pinning force as  $k_p = p/l_p$ , where  $l_p$  is the effective length of interaction of the vortex with pinning centers. Then  $\mu_v$  is calculated by Eq. (6) as in the case without pinning.

The points in Fig. 6 are the calculated values of the vibrational permeability  $\mu_v$  as a function of the pinning force for the parameters  $\kappa = 100$ ,  $l_p = 0.02 = 2\xi$  (where  $\xi$  is the coherence length), and different  $N_r$  values. It is seen that the interaction of vortices with pinning centers significantly reduces  $\mu_v$ , and the results of the calculation strongly depend on  $N_r$  up to a quite large value of  $N_r = 50$ . The effect of  $N_r$  is particularly strong at small  $p$  values. At  $N_r > 50$ , numerical calculations and achievement of a steady-state solution are too complicated. It is necessary to analytically analyze the considered phenomenon. The corresponding calculations are cumbersome and given in Appendices A and B. The final expressions for the distance to the first row and for the vibrational contribution to the permeability are presented below.

The distance to the first vortex row is given by the expression

$$\alpha_1 = \frac{\sqrt{\alpha_0}}{1 \pm \tilde{p}\alpha_0} \left[ \frac{h}{\tilde{b}_v} - \sqrt{\left(\frac{h}{\tilde{b}_v}\right)^2 - 1 + \tilde{p}^2 \pm 2\tilde{p} \sinh(d_{\text{eq}})} \right], \quad (23)$$

where  $\tilde{p} = p/[\tilde{b}_v \cosh(d_{\text{eq}}/2)]$ , and the upper and lower signs correspond to decreasing and increasing external fields, respectively. It is seen that the shift of the first row depends on the sign of pinning: it is larger in the case of decreasing field.

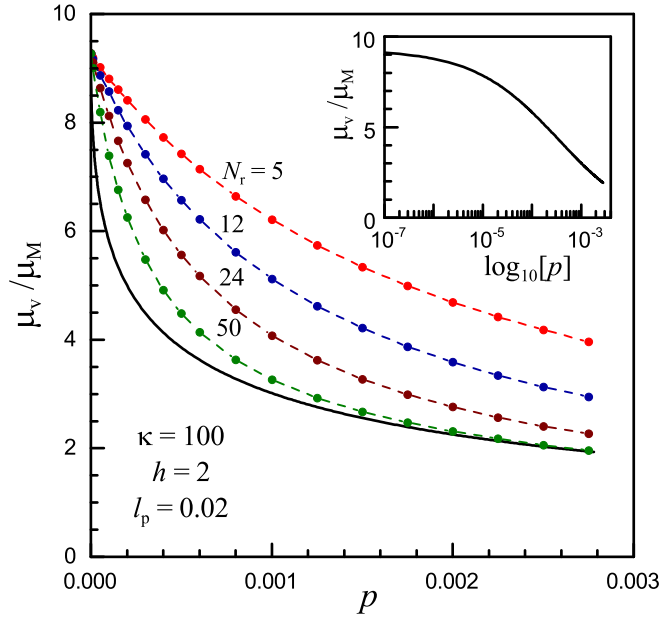


FIG. 6. Vibrational contribution to the permeability vs the pinning force. The dashed line is the numerical calculation with different numbers of exactly balanced rows  $N_r$ . The solid line is the calculation by Eq. (24). The inset shows the calculated curve in the lin-log scale.

The expression for the vibrational contribution to the permeability has the form

$$\mu_v = \mu_M \frac{2\alpha_1^2 [1 - 2\tilde{k}_p \alpha_0 (\sqrt{1 + \tilde{k}_p^{-1}} - 1) / (\alpha_0 - \alpha_1^2)]}{\alpha_0 - \alpha_1^2 [1 + 4\tilde{k}_p \alpha_0 / (\alpha_0 - \alpha_1^2)]}, \quad (24)$$

where

$$\tilde{k}_p = \frac{p \cosh(d_{\text{eq}}/2)}{l_p \tilde{b}_v}. \quad (25)$$

It is easy to verify that Eqs. (23) and (24) with  $p = 0$  have the form of Eqs. (16) and (19) for the unpinned vortex system, respectively.

Unlike Eq. (16), the denominator in Eq. (23) can be zero for the increasing field regime. In this regime, the pinning force is directed to the surface and impedes the penetration of vortices inside the superconductor. Pinning can completely prevent the penetration of vortices at large  $p$  values. Indeed, estimates indicate that this effect is possible in fields slightly above  $H_{c1}$ . However, at  $H \gg H_{c1}$ , the condition  $p(d_{\text{eq}}/2) \ll 1$ , which is necessary for the stability of the first row of vortices, is satisfied at all real parameters of HTSC crystals.

We now consider in more detail the singularities of Eq. (24) for the vibrational permeability. The numerator and denominator of this expression vanish at the force constant  $\tilde{k}_p = \tilde{k}_{p,c}$ , where

$$\tilde{k}_{p,c} = \frac{(\alpha_0 - \alpha_1^2)^2}{4\alpha_0 \alpha_1^2}. \quad (26)$$

Numerically,  $k_{p,c} \sim 0.01$ , which corresponds to the pinning force  $f_{p,c} \sim 10^{-4}$  under the assumption that  $l_p \sim \xi$ . It is easy to show that the quantity  $\mu_v(\tilde{k}_p)$  at  $\tilde{k}_p = \tilde{k}_{p,c}$  does not

have singularities and is given by the expression

$$\mu_v(\tilde{k}_{p,c}) = \mu_v(p=0) \frac{\alpha_1^2}{\alpha_0 + \alpha_1^2}, \quad (27)$$

which is about half the  $\mu_v$  value without pinning. These conclusions are in good agreement with the data shown in the inset of Fig. 6.

The value  $\tilde{k}_{p,c}$  separates the weak and strong pinning regions. The effect of pinning at  $\tilde{k}_p \ll \tilde{k}_{p,c}$  is insignificant, and the structure and low-frequency dynamics of the vortex lattice are determined by the interactions of vortices with each other and with the surface. In the opposite limit  $\tilde{k}_p \gg \tilde{k}_{p,c}$ , pinning becomes the leading factor and Eq. (24) can be represented in the form

$$\mu_v = \mu_M \tilde{k}_p^{-1/2}. \quad (28)$$

After the transition to dimensional quantities, this expression acquires the form

$$\mu_v = \frac{2\lambda_{\text{ac}}}{D}, \quad \text{where } \lambda_{\text{ac}}^2 = \frac{B\Phi_0}{4\pi k_p}, \quad (29)$$

which coincides with the expression for the Campbell penetration depth, where the force constant is given per unit length of the vortex.

The comparison of calculations by Eqs. (23)–(25) with the numerical calculations shows that the maximum difference is observed at weak pinning forces, i.e., in the region of transition from the free vortex lattice to the pinned one (see Fig. 6). It is shown in Appendix B that the amplitude of vortex vibrations decreases exponentially with an increase in the distance from the surface, and this decrease is faster for a stronger pinning force [see Eq. (B12)]. Apparently, for the parameters of the calculated curves in Fig. 6 in the region of weak pinning, the number of rows whose vibrations effectively contribute to  $\mu_v$  is larger than 50, whereas this number at  $p > 0.002$  is  $N_r < 50$ .

In the further consideration, we use only the analytical description of  $\mu_v(h, p, l_p)$  by Eq. (24). The inset of Fig. 6 shows in the lin-log scale how  $\mu_v$  decreases with increasing  $p$ . This plot makes it possible to determine the threshold value  $p \sim 10^{-5}$ , beginning with which pinning strongly affects  $\mu_v$ . An estimate of  $J_c \sim 2 \times 10^3$  A/cm<sup>2</sup> is obtained for the corresponding critical current density from Eq. (21) with the parameters  $\kappa = 70$  and  $\lambda = 0.2 \mu\text{m}$  typical of the YBaCuO HTSC. This low current for HTSC crystals usually occurs at the temperatures near  $T_c$ , so that the effect of pinning on vibrational vortex motion can be neglected only in this narrow temperature range.

Figure 7 shows the dependences  $\mu_v(h)$  in increasing and decreasing dc fields at different parameters  $l_p$ . At large  $l_p > 5\xi$ , i.e., for a sufficiently smooth potential well, the effect of pinning on the amplitude of vibrations is not too strong, and the direction of the shift of the vortex rows nearest to the surface, which is determined by the direction of the variation of the dc field, is pronounced. However, as  $l_p$  decreases to the most physically reliable value  $l_p \sim \xi$ , the pinning well becomes narrow, so that the effect of pinning is reduced primarily to a decrease in both the amplitude of vibrations and



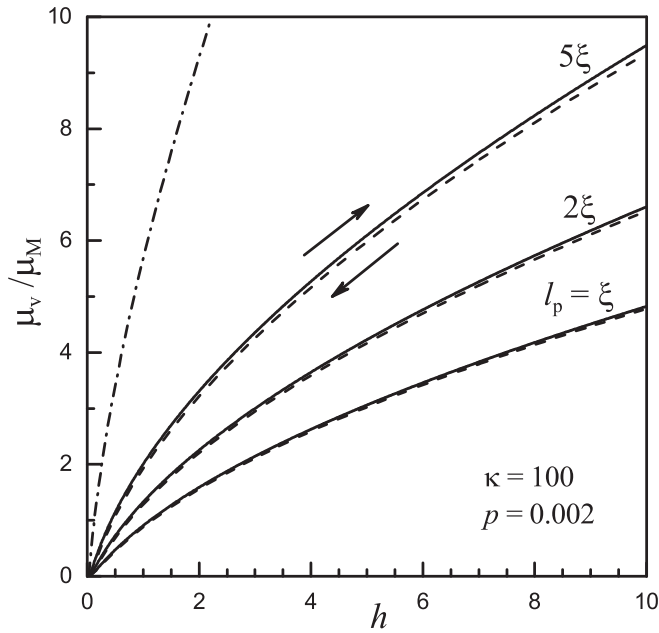


FIG. 7. Field dependences of the contribution from the vibrations of the pinned vortex lattice to the permeability at different lengths of interaction of vortices with pinning centers  $l_p$  in units of the coherence length in the case of (solid lines) increasing and (dashed lines) decreasing fields. The dash-dotted line is a similar dependence in the absence of pinning.

$\mu_v$ . In this case, the position of the vortex inside the well can affect  $\mu_v$  only because of the deviation of the shape of the well from parabolic and the corresponding change in  $k_p$ . This effect was observed in cuprate HTSCs with a high degree of anisotropy [15,16].

### III. EXPERIMENT

A thin superconducting plate in an external magnetic field parallel to its flat surface is geometrically most appropriate for the experimental study of vibrational vortex motion. In this case, the vortex structure is parallel to the surface, and the demagnetizing factor is negligibly small. In this paper, the measurements were performed with the YBaCuO HTSC, which was split from an oriented massive crystal grown by the method described in Ref. [41]. The plate sample had the sizes  $L \times W \times D = 4.0 \times 1.8 \times 0.29$  mm, where  $L$  and  $W$  are the length and width of the flat face (which is parallel to the crystallographic  $ab$  plane), respectively, and  $D$  is the thickness. The condition  $D \gg \lambda$  was valid at all temperatures. The sample was additionally saturated with oxygen at 360 °C during 267 h in an oxygen flow. The onset temperature of the superconducting transition was 88 K. Figure 8 shows the x-ray diffraction pattern ( $\text{CuK}\alpha$  radiation) obtained at reflection from the flat face of the single crystal. It is seen that this diffraction pattern contains only  $(00l)$  reflections, which indicates a pronounced anisotropy with the direction along the  $c$  axis perpendicular to the flat face. The lattice parameter  $c = 11.675$  Å is slightly smaller than the value  $c = 11.69$  Å in good samples with the oxygen content  $y = 6.92$  [42]. This

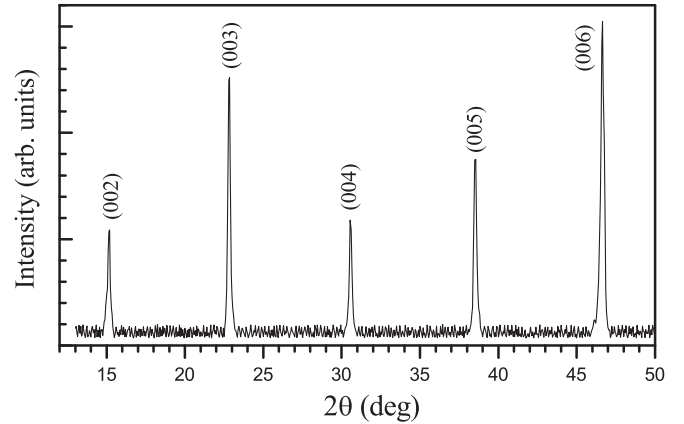


FIG. 8. X-ray diffraction pattern of the studied  $\text{YBa}_2\text{Cu}_3\text{O}_y$  single crystal.

difference can be due to slight oxygen overdoping or a small impurity of light elements existing in YBaCuO single crystals.

The response of the sample to the ac magnetic field was measured on a specially designed setup that is based on the two-coil method and has sufficiently high stability and sensitivity to detect small changes in the dependence on the dc field. The ac field has a frequency of 980 Hz, and the amplitude varied in the range  $H_m = 0.1\text{--}20$  Oe. The dc field generated by a copper solenoid placed in liquid nitrogen varied in the range of 0–2.5 kOe. The dc and ac magnetic fields were directed along the long edge of the single-crystal plate. First, we measured the field dependences of the real and imaginary parts of the magnetic susceptibility. The susceptibility was normalized to the value measured in zero dc magnetic field at  $T = 70$  K and  $H_m = 0.1$  Oe. Then these results were recalculated to the permeability because it better describes the penetration of the ac field into the sample.

Figure 9 shows the field dependences of the real and imaginary parts of the permeability measured at 81.0 K. Similar data were also obtained at different temperatures. It is seen that the real part of the permeability  $\mu'$  increases monotonically with both the dc field and the amplitude of the ac field, which indicates an increase in the effective volume into which the ac magnetic field penetrates. Losses on magnetization reversal, which are characterized by the imaginary part of the permeability  $\mu''$ , also increase.

As seen in Fig. 9, in addition to the amplitude-independent (linear) contributions of  $\mu_M$  and  $\mu_v$  to the permeability considered above, there is a contribution depending on the amplitude. This nonlinear contribution is due to the entry-exit of vortices into-from the sample in the process of modulation of the external field by the ac component. The amplitude dependences of  $\mu'$  at  $T = 81$  K and various dc fields are shown in the inset of Fig. 9, where the procedure of separation of the contributions is also demonstrated. The extrapolation of the dependence  $\mu'(H_m)$  to  $H_m = 0$  gives the sum  $\mu_M + \mu_v$ , where the term  $\mu_M$  corresponds to zero dc field. It is seen that changes in  $\mu'$  appear beginning with the smallest amplitudes and are close to linear. As known, such an amplitude dependence is characteristic of the contribution  $\mu'_c$  caused by

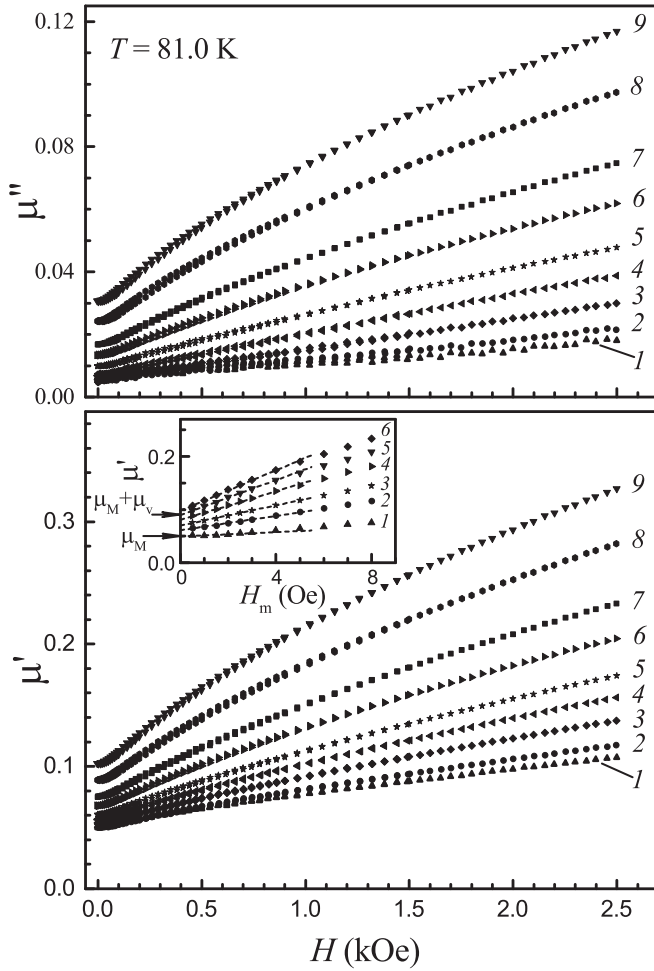


FIG. 9. Field dependences of the real ( $\mu'$ ) and imaginary ( $\mu''$ ) parts of the permeability of the YBaCuO single crystal at  $T = 81$  K and amplitudes of the ac field  $H_m = (1)$  0.5, (2) 1.0, (3) 2.0, (4) 3.0, (5) 4.0, (6) 6.0, (7) 8.0, (8) 12.0, and (9) 16.0 Oe. Inset: Amplitude dependences of the real part  $\mu'$  of the permeability of the YBaCuO single crystal at  $T = 81$  K and  $H = (1)$  0, (2) 0.5, (3) 0.9, (4) 1.5, (5) 2.0, and (6) 2.5 kOe.

the implementation of the critical state if the ac field does not reach the center of the sample (see, e.g., Refs. [21,43]).

A reason for the possibility of the vibrations of vortices and their macroscopic shift with the formation of the critical state simultaneously occurring was studied in Ref. [44]. The effect of the thickness  $D$  of the single crystal, which was successively reduced by means of grinding, on  $\mu_v$  and  $\mu'_c$  was revealed. It was found that  $\mu_v$  increases inversely proportional to  $D$ , whereas changes in  $\mu'_c$  are small. This result shows that the simultaneous occurrence of reversible and irreversible vortex motions is due to a high anisotropy of the properties of the HTSC single crystal in the external field directed along structure layers. Two types of vortex motion are spatially separated: vortices vibrate near the flat face of the plate in the direction of the  $c$  axis, whereas the entry and exit of vortices occur along structure layers through the crystal.

Thus, the analysis of the amplitude dependences of  $\mu'$  makes it possible to separate two types of vortex motion and to determine the corresponding characteristics  $\mu_v$  and  $J_c$ . The

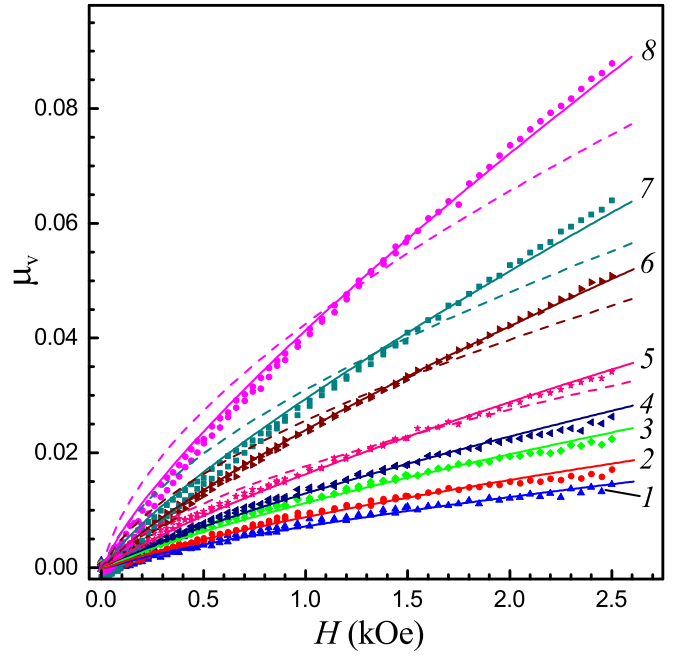


FIG. 10. Field dependences of the contribution from the vibrations of vortices along the  $c$  axis to the permeability of the YBaCuO single crystal (points) at  $T = (1)$  73.6, (2) 75.9, (3) 78.0, (4) 79.0, (5) 80.0, (6) 81.0, (7) 81.5, and (8) 82.0 K. Calculated curves (dashed lines) without pinning and (solid lines) considering the pinning are also shown.

critical current density was calculated from the slope of the linear segment of  $\mu'(H_m)$  using the relation [21,43]

$$\mu'_c(H_m) = H_m \left( \frac{5}{2\pi J_c W} \right). \quad (30)$$

Here,  $J_c$  is the critical current density in A/cm<sup>2</sup>,  $W$  is the sample dimension in the direction of penetration of the ac field in centimeters, and  $H_m$  is the amplitude of the ac magnetic field in oersteds.

The amplitude dependences of magnetic losses also confirm the implementation of the critical state. The corresponding imaginary part of the permeability in the low-frequency limit is given by the expression

$$\mu''(H_m) = \mu''_c(H_m) = H_m \left( \frac{10}{3\pi^2 J_c W} \right). \quad (31)$$

Indeed, the experimental dependences  $\mu''(H_m)$  are almost linear, and the ratio of the slopes of  $\mu'(H_m)$  and  $\mu''(H_m)$  is very close to a value predicted by Eqs. (30) and (31).

The vibrational permeability and critical current density thus obtained as functions of the dc magnetic field are shown in Figs. 10 and 11, respectively. It is seen that the vibrational permeability  $\mu_v$  increases with both the magnetic field  $H$  and temperature. This behavior reflects both an increase in the vortex density with the magnetic field  $H$  and a decrease in the elastic constants of the vortex lattice with increasing temperature. The field dependences of the inverse critical current density shown in Fig. 11 demonstrate that  $J_c$  decreases monotonically with an increase in both the temperature and the dc magnetic field.

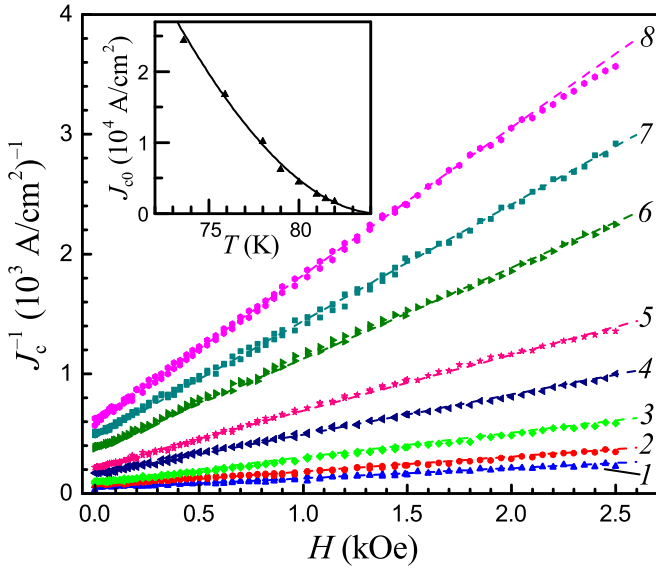


FIG. 11. Field dependences of the inverse critical current density (the pinning force is directed along the  $ab$  layers) for the YBaCuO single crystal. Lines 1–8 correspond to the same temperatures as the respective lines in Fig. 10. The inset shows the temperature dependence of  $J_c(H=0)$ , where the solid line is the calculation by Eq. (36).

#### IV. DISCUSSION

To compare the results of calculations with experimental data, it is necessary to relate dimensionless quantities in the resulting formulas to the physical characteristics of the sample. Since the external field is directed along structure layers, the anisotropy of the magnetic properties of the HTSC should be considered. As known, the degree of anisotropy is determined by the ratio  $\gamma = \lambda_c/\lambda_{ab} = \xi_{ab}/\xi_c$ , where  $\lambda_{ab}$  and  $\lambda_c$  ( $\xi_{ab}$  and  $\xi_c$ ) are the components of the London penetration depth (coherence length). An exception is the thermodynamic critical field, which is independent of the orientation of the external field with respect to the axes of the crystal and relates the magnetic induction (or the magnetic field) to its dimensionless analog:

$$B(H) = \sqrt{2}H_c b(h) = \frac{\kappa_c \Phi_0}{2\pi \lambda_{ab}^2} b(h). \quad (32)$$

Vibrations of vortices occur in the direction of the  $c$  axis; consequently,

$$\mu_M = \frac{2\lambda_{ab}}{D}, \quad (33)$$

and  $\kappa = \gamma\kappa_c$  should be substituted into Eq. (13) to calculate the thermodynamic potential.

The calculation of  $\mu_v(H)$  should include the pinning force directed along the  $c$  axis; additional investigations are required to determine the magnitude of this force. For this reason, as a start point,  $\mu_v(H)$  is calculated in the limit of negligibly small pinning. If the parameters  $\kappa_c = 70$  and  $\gamma = 5$  typical of the YBaCuO HTSC are used, the London penetration depth  $\lambda_{ab}$  is the only fitting parameter in Eqs. (16)–(20) at each temperature in this case. The calculated curves are shown by the dashed lines in Fig. 10. It is seen that they poorly describe

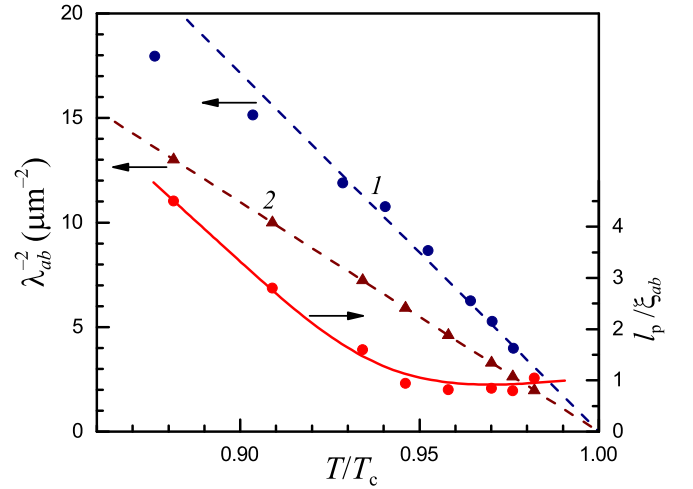


FIG. 12. Temperature dependences of (dashed lines, left axis) the inverse square of the London penetration depth  $\lambda_{ab}$  (1) calculated without pinning by fitting Eq. (19) to experimental data and (2) calculated values used to determine the contribution of pinning to  $\mu_v(H)$  curves and (solid line, right axis) the effective length of interaction of vortices with pinning centers  $l_p$  in units of the coherence length  $\xi_{ab}$ .

the experimental dependences, and the discrepancy becomes more pronounced as the temperature increases and approaches  $T_c$ . In addition, the corresponding  $\lambda_{ab}(T)$  values (Fig. 12) are not reliable. First, they are noticeably smaller than the literature data (see, e.g., Ref. [45]). Second, the dependence  $\lambda_{ab}^{-2}(T)$  deviates from an expected linear law in the studied narrow temperature range near  $T_c$ . This behavior of  $\lambda_{ab}(T)$  was predicted in Ref. [46] and was experimentally confirmed in Refs. [45,47] for the YBaCuO HTSC with different degrees of inhomogeneity.

We now consider the effect of the field-dependent pinning force on the calculated  $\mu_v(H)$  curves. The pinning force entering Eqs. (23) and (24) corresponds to the critical current density  $J_{c,ab}$  flowing along the  $ab$  plane. Being the refinement of Eq. (21), the corresponding relation has the form

$$p = \frac{4\pi^2 \lambda_{ab}^3}{5\kappa_c \Phi_0} J_{c,ab}. \quad (34)$$

The layered structure of the system can be responsible for the anisotropy of the pinning force corresponding to the anisotropy of critical currents along and across structure layers. This problem is beyond the scope of this paper. It is only noteworthy that the study in Ref. [48] of mechanisms of pinning in the YBaCuO single crystal revealed the dominant role of point defects (isotropic mechanism of pinning) compared with intrinsic pinning (which is strongly anisotropic) near  $T_c$ . For this reason, the measured  $J_c(H)$  dependences are used in the calculations by Eq. (34). As seen in Fig. 11, these dependences are well described by the known Kim-Anderson model [49,50]:

$$J_c(H) = \frac{J_{c0}}{(1 + H/B_0)}. \quad (35)$$

It is remarkable that the parameter  $B_0 = 480$  Oe determined by the fitting of Eq. (35) to the experimental data

is the same within the error for different temperatures. This value of the magnetic induction corresponds to the intervortex distance  $a \approx \sqrt{\Phi_0/B_0} \approx 0.2 \mu\text{m}$  and, according to Ref. [50], characterizes the size of the flux bundle.

The temperature dependences of the critical current density  $J_{c0}$  in zero external field are shown in the inset of Fig. 11 and are well described by the formula [51]

$$J_{c0} = J_{c0}(T = 0) \left[ 1 - \left( \frac{T}{T_c} \right)^2 \right]^m. \quad (36)$$

with the parameters  $J_{c0}(T = 0) = 4.3 \times 10^5 \text{ A/cm}^2$  and  $m = 2$ .

The length of interaction  $l_p$  of vortices with pinning centers is also an unknown parameter in the calculations. To determine  $l_p$ , we perform the calculations at given  $\lambda_{ab}(T)$  values close to the literature data [45]. Figure 12 shows the used  $\lambda_{ab}$  values (line 2), which are described by the empirical dependence  $\lambda_{ab}^{-2} = 2\lambda_0^{-2}(1 - T/T_c)$ , where  $\lambda_0 = 0.135 \mu\text{m}$  is the London penetration depth at  $T = 0$ . The resulting dependences  $\mu_v(H)$  are shown by the solid lines in Fig. 10. As seen, the inclusion of pinning makes it possible to obtain good agreement of the calculated curves with the experimental data. This agreement is due to a decrease in the pinning force with increasing field, which leads to the straightening of the calculated  $\mu_v(H)$  curves. It is interesting that the resulting  $l_p$  values are close to the coherence length  $\xi_{ab}$  (see Fig. 12) despite many assumptions. Another interesting result is an increase in  $l_p$  with decreasing temperature, which can be due to an increase in the rigidity of the vortex lattice.

## V. CONCLUSIONS

The reported numerical and analytical calculations of the properties of the vortex lattice near the surface of a type-II superconductor in a magnetic field oriented along the surface provide the following results.

(i) The accuracy of the description of intervortex interactions, which depends on the model of the structure of the vortex core, affects the calculated positions of vortex rows and the amplitudes of their reversible vibrations induced by the external ac magnetic field. However, the contribution  $\mu_v$  of this process to the permeability is model independent.

(ii) It is important that the analytical expressions in Eqs. (23) and (24) have been derived for the distance from the surface to the nearest row and the vibrational permeability  $\mu_v$ , respectively, as functions of the parameters of the superconductor ( $\lambda$ ,  $\kappa$ ,  $F_p$ ,  $k_p$ ) and the dc field. Calculations have been performed for the discrete vortex lattice, including the interactions of vortices with each other, with the surface, and with pinning centers.

(iii) A method for the experimental determination of  $\mu_v$  from the amplitude dependences of the real part of the permeability has been proposed. The developed theoretical approaches have been applied to describe data for the YBaCuO HTSC single crystal in the external magnetic field parallel to structure layers. It has been shown that the field dependence of the parameters of the effective interaction potential of vortices with pinning centers should be considered to achieve good agreement between the calculated and experimental  $\mu_v(H)$  curves.

(iv) The derived relations allow the determination of the effective length of interaction of vortices with pinning centers by means of the joint analysis of experimental data for the magnetodynamic response and the critical current density.

It is noteworthy that Eq. (24) is valid in a wide range of the elastic constant  $k_p$  characterizing the slope of the pinning potential well. In particular, Eq. (24) remains valid in the case of weak pinning (e.g., near the irreversibility line), where the classical Campbell approach is inapplicable. In this case, it is necessary to consider the proximity of the surface in addition to pinning effects when describing reversible vortex vibrations. In the presence of even a low surface potential barrier, the amplitude of vibrations  $a_m(x)$ , as well as  $\mu_v$ , remains finite even in the absence of pinning.

It is also remarkable that an exponential decrease in  $a_m(x)$  with an increase in the distance from the surface has been obtained both within the discrete model and in the continuum approximation, i.e.,  $a_m(x)$  is described by the same function as the driving force generated by the Meissner current. However, the scale of spatial variation of the driving force is constant (London penetration depth), whereas the scale of variation for the amplitude of vibrations depends on the relation between the elastic coupling constant of vortices with pinning centers and the magnetic induction [see Eq. (B12)]. The latter scale can vary in a wide range and can be much larger than  $\lambda$ .

The results obtained in this paper can be useful for determining the parameters of the pinning energy landscape. This information is of particular significance for oriented HTSC films, which are used to fabricate second-generation HTSC wires. The results obtained for the single crystal are completely applicable for these objects in the external magnetic field parallel to the surface. The joint analysis of the field dependences of the low-frequency permeability and the critical current density makes it possible to obtain quantitative information on the depth and effective size of the pinning potential well. These data are important for seeking the most efficient types of pinning centers to increase the critical current of HTSC materials.

## ACKNOWLEDGMENTS

I am grateful to O. K. Karyagina for obtaining x-ray data for the single crystal and to A. I. Shushin for stimulating discussions. This paper was supported by the Russian Federal Agency for Scientific Organizations (State Task No. 0082-2018-0003, Registration No. AAAA-A18-118012390045-2) and by the Russian Foundation for Basic Research (Project No. 17-29-10016).

## APPENDIX A: POSITIONS OF VORTEX ROWS

To determine the equilibrium positions of vortex rows in the presence of pinning, it is necessary to solve the system of Eq. (3). To reduce formulas, we introduce the dimensionless variables

$$h' = \frac{\kappa ah}{\pi}, \quad f'_p = \frac{\kappa a f_p}{\pi}. \quad (A1)$$

Then the force balance conditions in Eq. (3) for a vortex in the  $n$ th row in the EA acquires the form

$$h' \exp(-x_n) + \sum_{i=1}^{n-1} \exp(x_i - x_n) - \sum_{i=n+1}^N \exp(x_n - x_i) - \sum_{i=1}^N \exp(-x_i - x_n) + f'_p = 0, \quad (\text{A2})$$

(the pinning force is negative for an increasing dc field and is positive for a decreasing dc field). The total number  $N$  of rows considered should be quite large ( $Nd_{\text{eq}} \gg 1$ ) and, as shown below, does not enter the final formulas. Further, we use a mathematical trick proposed in Ref. [52] to describe a vortex structure in an inhomogeneous Josephson junction. Later, it was successfully applied to calculate the vortex structure in a hard superconductor [53]. Following those papers, we introduce the auxiliary variables

$$\alpha_n = \exp(-x_n + x_{n-1}), \quad n \geq 2, \quad (\text{A3})$$

$$K_1 = 0, \quad K_{i+1} = \alpha_{i+1}(1 + K_i), \quad (\text{A4})$$

$$G_{N+1} = 0, \quad G_i = \alpha_i(1 + G_{i+1}), \quad (i = 1 \dots N). \quad (\text{A5})$$

As a result, the balance condition in Eq. (A2) acquires the form

$$K_n - G_{n+1} + \alpha_1 \dots \alpha_n (h' - G_1) + f'_p = 0. \quad (\text{A6})$$

Further, the summation of Eq. (A6) from  $n = k$  to  $N$  in Ref. [53] gave an equation including  $N$ . Such an approach is hardly applicable to calculate the vortex lattice near the surface; for this reason, we modify it and sum Eq. (A6) from  $n = 1$  to  $k \geq 2$ :

$$G_{k+1}(K_k + 1) - (G_1 - \alpha_1 \dots \alpha_k G_{k+1})(h' - G_1) - k f'_p = 0. \quad (\text{A7})$$

The joint solution of the system of Eq. (A6) with  $n = k$  and Eq. (A7) leads to a quadratic equation for  $G_{k+1}$ , which has the solution

$$G_{k+1} = -\frac{1 - f'_p}{2} + \frac{1}{2} \sqrt{(1 - f'_p)^2 + 4G_1(h' - G_1) + 4k f'_p}. \quad (\text{A8})$$

Cases of Eq. (A5) for  $i = 1, 2$  together with Eq. (A8) for  $k = 2, 3$  and with the previously introduced boundary condition in Eq. (22), which in the accepted notation has the form  $\alpha_2 = \alpha_0$ , constitute a closed system of equations. Its solution gives the following formula for the distance from the surface to the first vortex row:

$$\alpha_1 = \frac{h' - \sqrt{h'^2 + 4f'_p - A}}{1 + f'_p + \sqrt{(1 - f'_p)^2 + A}}, \quad (\text{A9})$$

where

$$A = 4\alpha_0 \left[ \frac{1}{(1 - \alpha_0)^2} - f_p'^2 \frac{1}{(1 + \alpha_0)^2} \right]. \quad (\text{A10})$$

Further, passing from  $h'$  and  $f'_p$  back to  $h$  and  $f_p$  and considering Eq. (17), one can transform Eq. (A9) to Eq. (23).

## APPENDIX B: VIBRATIONAL CONTRIBUTION TO THE PERMEABILITY

As mentioned above, the permeability  $\mu_v$  is determined by both the positions of vortex rows and their shift  $\delta x_n$  under a small variation of the external field  $\delta h$ . To calculate  $\delta x_n$ , it is necessary to add an elastic returning force to the force balance conditions:

$$(h' + \delta h') \exp(-x_n - \delta x_n) + \sum_{i=1}^{n-1} \exp(x_i + \delta x_i - x_n - \delta x_n) - \sum_{i=n+1}^N \exp(x_n + \delta x_n - x_i - \delta x_i) - \sum_{i=1}^N \exp(-x_i - \delta x_i - x_n - \delta x_n) + f'_p - k'_p \delta x_n = 0, \quad (\text{B1})$$

where  $k'_p = f'_p/l_p$ .

Expanding Eq. (B1) in small parameters  $\delta x_i$  and  $\delta h'$ , considering Eq. (A2), and using the introduced variables, we obtain

$$\begin{aligned} & \delta h' \exp(-x_n) + \delta x_n [-G_{n+1} - K_n - \alpha_1 \dots \alpha_n (h' - G_1) - k'_p] \\ & + \sum_{i=1}^{n-1} \delta x_i \exp(x_i - x_n) \\ & + \sum_{i=n+1}^N \delta x_i \exp(x_n - x_i) \\ & + \exp(-x_n) \left[ 1 + \sum_{i=1}^N \delta x_i \exp(-x_i) \right] = 0. \quad (\text{B2}) \end{aligned}$$

To further simplify Eq. (B2), we substitute the expression for  $K_n$  from Eq. (A6), multiply by  $\exp(-x_n) = \alpha_1 \dots \alpha_n$ , and introduce the variables

$$\beta_n = \alpha_1 \dots \alpha_n \frac{\delta x_n}{\delta h'}. \quad (\text{B3})$$

As a result, Eq. (B2) is transformed to

$$\begin{aligned} & \beta_n (2G_{n+1} + 1 - f'_p + k'_p) \\ & = \sum_{i=1}^{n-1} \beta_i (\alpha_{i+1} \dots \alpha_n)^2 \\ & + \sum_{i=n+1}^N \beta_i + (\alpha_1 \dots \alpha_n)^2 \left( 1 + \sum_{i=1}^N \beta_i \right). \quad (\text{B4}) \end{aligned}$$

Up to a constant factor, the variables  $\beta_n$  are the terms of the sum in Eq. (6) determining  $\mu_v$ . It is easy to verify that

$$\frac{\mu_v}{\mu_M} = 2X, \quad (\text{B5})$$

where

$$X = \sum_{n=1}^{\infty} \beta_n. \quad (\text{B6})$$

The numerical calculations showed that the effect of pinning on the permeability  $\mu_v$  is due to the variation of the distance from the surface to the nearest row and to a decrease in the amplitude of vortex vibrations. At the same time, the effect of variation of the distances between rows (magnetic field gradient) is insignificant. For this reason, the difference of the distances between the rows from the equilibrium value is neglected, i.e.,  $\alpha_n = \alpha_0$  ( $n \geq 2$ ). In addition,  $f'_p$  in Eq. (B4) for superconductors with  $\kappa \gg 1$  can be neglected compared with  $k'_p$  because  $k'_p \sim \kappa f'_p$ . Then Eq. (B4) in the limit  $N \rightarrow \infty$  acquires the form

$$\beta_n \left[ \frac{1 + \alpha_0}{1 - \alpha_0} + k'_p \right] = X + \alpha_1^2 \alpha_0^{2(n-1)} (X + 1) - \sum_{i=1}^{n-1} \beta_i [1 - \alpha_0^{2(n-i)}]. \quad (\text{B7})$$

$$X = \frac{\alpha_1^2 [2(\alpha_0 - \alpha_1^2) + k'_p(1 - \alpha_0^2)] - \sqrt{k_p'^2(1 - \alpha_0^2)^2 + 4k'_p\alpha_0(1 - \alpha_0^2)}}{2[(\alpha_0 - \alpha_1^2)^2 - k_p'\alpha_1^2(1 - \alpha_0^2)]}. \quad (\text{B10})$$

This formula acquires the form of Eq. (24), if Eq. (B5) is considered and  $k'_p$  is changed to  $k_p$  according to

$$k'_p = \frac{f'_p}{l_p} = \left( \frac{f_p}{l_p} \right) \frac{\kappa a}{\pi} = k_p \frac{\kappa a}{\pi} = k_p \frac{2\sqrt{\alpha_0}}{\tilde{b}_v(1 - \alpha_0)}. \quad (\text{B11})$$

The choice of the trial function for  $\beta_n$  is one of the most unobvious steps in the solution of this problem. This function should satisfy the physical requirement of the exponential decrease in the amplitude of vortex vibrations with an increase in the distance to the surface. This requirement is imposed

The general solution of Eq. (B7) will be sought with the trial function

$$\beta_n = X(1 - y)y^{n-1}. \quad (\text{B8})$$

It is easy to verify that this function satisfies Eq. (B6). Equation (B7) is valid at any  $n$  values if

$$X(1 - y) \left[ \frac{1 + \alpha_0}{1 - \alpha_0} + k'_p \right] - X = \alpha_1^2(1 + X),$$

$$\alpha_1^2(1 + X) + \frac{X(1 - y)\alpha_0^2}{(\alpha_0^2 - y)} = 0. \quad (\text{B9})$$

The solution of this system of equations finally gives

because the external force generating the vibrations of vortices is due to the Meissner current and decreases exponentially with an increase in the distance from the surface. According to Eqs. (B3) and (B8),

$$\delta x_n = \delta x_1 \exp[(n - 1)(d_{\text{eq}} + \ln y)]. \quad (\text{B12})$$

In the absence of pinning,  $y = \alpha_0$ ,  $\delta x_n = \delta x_1$ , and the vortex lattice vibrates as a whole. In the case of pinning,  $y < \alpha_0$ , and the amplitude of the vibrations of vortices decreases exponentially with an increase in  $n$ .

- [1] A. M. Campbell, The response of pinned flux vortices to low-frequency field, *J. Phys. C* **2**, 1492 (1969).
- [2] A. M. Campbell, The interaction distance between flux lines and pinning centres, *J. Phys. C: Solid St. Phys.* **4**, 3186 (1971).
- [3] E. H. Brandt, Penetration of Magnetic ac Fields into Type-II Superconductors, *Phys. Rev. Lett.* **67**, 2219 (1991).
- [4] E. H. Brandt, Superconductor disks and cylinders in an axial magnetic field: II. Nonlinear and linear ac susceptibilities, *Phys. Rev. B* **58**, 6523 (1998).
- [5] M. W. Coffey and J. R. Clem, Theory of rf magnetic permeability of isotropic type-II superconductors in a parallel field, *Phys. Rev. B* **45**, 9872 (1992).
- [6] J. R. Clem and M. W. Coffey, Vortex dynamics in a type-II superconducting film and complex linear-response functions, *Phys. Rev. B* **46**, 14662 (1992).
- [7] T. Matsushita, E. S. Otabe, and B. Ni, Effect of reversible fluxoid motion on ac susceptibility of high temperature superconductors, *Physica C* **182**, 95 (1991).
- [8] A. E. Koshelev and V. M. Vinokur, Frequency response of pinned vortex lattice, *Physica C* **173**, 465 (1991).
- [9] C. J. van der Beek, V. B. Geshkenbein, and V. M. Vinokur, Linear and nonlinear ac response in the superconducting mixed state, *Phys. Rev. B* **48**, 3393 (1993).
- [10] E. S. Otabe, R. Kitamura, and T. Matsushita, ac susceptibility measurements for superconducting Y-Ba-Cu-O powder, *Jpn. J. Appl. Phys.* **35**, 6023 (1996).
- [11] H. Kawamura, T. Fujiyoshi, and K. Miyahara, Temperature dependences of the critical current density and the pinning potential near the irreversibility temperature in YBa<sub>2</sub>Cu<sub>3</sub>O<sub>7- $\delta$</sub> , *Supercond. Sci. Technol.* **8**, 806 (1995).
- [12] G. Pasquini and V. Bekeris, Peak effect in YBCO crystals: statics and dynamics of the vortex lattice, *Supercond. Sci. Technol.* **19**, 671 (2006).
- [13] E. Bartolome, A. Palau, A. Llordés, T. Puig, and X. Obradors, Vortex oscillations in TFA-grown YBCO thin-films with BZO nanoparticles, *Physica C* **470**, 2033 (2010).
- [14] Y. Fukumoto and T. Matsushita, The effect of reversible flux motion on the estimation of critical current density in a thin superconductor using a third harmonic voltage method, *Supercond. Sci. Technol.* **18**, 861 (2005).
- [15] R. Prozorov, R. W. Giannetta, N. Kameda, T. Tamegai, J. A. Schlueter, and P. Fournier, Campbell penetration depth of a superconductor in the critical state, *Phys. Rev. B* **67**, 184501 (2003).
- [16] R. Willa, V. B. Geshkenbein, R. Prozorov, and G. Blatter, Campbell Response in Type-II Superconductors under Strong Pinning Conditions, *Phys. Rev. Lett.* **115**, 207001 (2015).

- [17] R. Willa, V. B. Geshkenbein, and G. Blatter, Campbell penetration in the critical state of type-II superconductors, *Phys. Rev. B* **92**, 134501 (2015).
- [18] R. Willa, V. B. Geshkenbein, and G. Blatter, Probing the pinning landscape in type-II superconductors via Campbell penetration depth, *Phys. Rev. B* **93**, 064515 (2016).
- [19] C. P. Bean and J. D. Livingston, Surface Barrier in Type-II Superconductors, *Phys. Rev. Lett.* **12**, 14 (1964).
- [20] F. F. Ternovskii and L. N. Shekhata, Structure of the mixed state near the boundary of a semi-infinite type II superconductor of the second kind, *Sov. Phys. JETP* **35**, 1202 (1972).
- [21] L. G. Mamsurova, K. S. Pigalskiy, V. P. Sakun, and L. G. Scherbakova, Hysteresis of the dynamical magnetic permeability of a  $\text{YBa}_2\text{Cu}_3\text{O}_{7-\delta}$  single crystal, *Physica C* **200**, 175 (1992).
- [22] L. G. Mamsurova, K. S. Pigalskiy, V. P. Sakun, and L. G. Scherbakova, Pinning and near-surface flux dynamics of the  $\text{YBaCuO}$  single crystal, *Physica C* **235–240**, 3225 (1994).
- [23] L. G. Mamsurova, K. S. Pigalskiy, V. P. Sakun, and L. G. Scherbakova, Structure and dynamics of vortex lattice near  $\text{YBaCuO}$  monocrystal surface, *Phys. Solid State* **37**, 1630 (1995).
- [24] K. I. Kugel, L. G. Mamsurova, K. S. Pigalskiy, and A. L. Rakhmanov, Surface barrier and magnetic hysteresis of ac permeability in  $\text{YBaCuO}$  single crystal, *Physica C: Supercond.* **300**, 270 (1998).
- [25] K. I. Kugel, A. L. Rakhmanov, L. G. Mamsurova, and K. S. Pigal'skii, Mixed state stability range in a  $\text{YBaCuO}$  single crystal, *Low Temp. Phys.* **24**, 617 (1998).
- [26] R. Laiho, M. Safonchik, and K. B. Traito, Labusch parameter of flux line lattice with planar pinning centers, *Physica C* **418**, 87 (2005).
- [27] L. G. Mamsurova, K. S. Pigalskiy, and W. V. Pogosov, Equilibrium magnetic characteristics of high- $T_c$  superconductors with allowance for the spatial distribution of the order parameter in the vortex cores. II. Vibrational contribution to the dynamic magnetic permeability, *Low Temp. Phys.* **27**, 119 (2001).
- [28] J. R. Clem, Simple model for the vortex core in a type II superconductor, *J. Low Temp. Phys.* **18**, 427 (1975).
- [29] Z. Hao, J. R. Clem, M. W. McElfresh, L. Civale, A. P. Malozemoff, and F. Holtzberg, Model for the reversible magnetization of high- $\kappa$  type-II superconductors: application to high- $T_c$  superconductors, *Phys. Rev. B* **43**, 2844 (1991).
- [30] V. V. Pogosov, A. L. Rakhmanov, and K. I. Kugel, Magnetization of type-II superconductors in the range of fields  $H_{c1} \leq H \leq H_{c2}$ : variational method, *JETP* **91**, 588 (2000).
- [31] W. V. Pogosov, K. I. Kugel, A. L. Rakhmanov, and E. H. Brandt, Approximate Ginzburg-Landau solution for the regular flux-line lattice: circular cell method, *Phys. Rev. B* **64**, 064517 (2001).
- [32] G. Carneiro and E. H. Brandt, Vortex lines in films: fields and interactions, *Phys. Rev. B* **61**, 6370 (2000).
- [33] V. V. Shmidt, Critical current of an ideal type II superconductor in the mixed state, *Sov. Phys. JETP* **34**, 211 (1972).
- [34] K. S. Pigal'skii and L. G. Mamsurova, Dynamic magnetic permeability of a thin, high- $T_c$  superconducting wafer, *Phys. Solid State* **39**, 1737 (1997).
- [35] A. S. Krasil'nikov, L. G. Mamsurova, N. G. Trusevich, L. G. Shcherbakova, and K. K. Pukhov, Reversible magnetization of fine-grained high- $T_c$  superconductors, *JETP* **82**, 542 (1996).
- [36] A. I. Rusinov and G. S. Mkrchyan, On the theory of the Abrikosov vortex lattice in superconductors with  $\kappa \gg 1$ , *Sov. Phys. JETP* **34**, 413 (1972).
- [37] C. R. Hu, Numerical constants for isolated vortices in superconductors, *Phys. Rev. B* **6**, 1756 (1972).
- [38] K. S. Pigalskiy, Mixed state and magnetization of a thin type II superconducting film in the applied parallel magnetic field: variational technique of the inclusion of the contribution from the core of a vortex, *JETP Lett.* **101**, 168 (2015).
- [39] V. V. Moshchalkov, J. Y. Henry, C. Marin, J. Rossat-Mignod, and J. F. Jacquot, Anisotropy of the first critical field and critical current in  $\text{YBa}_2\text{Cu}_3\text{O}_{6.9}$  single crystals, *Physica C* **175**, 407 (1991).
- [40] Y. Kimishima and Y. Ichiyanaagi, Magnetization analysis of high  $T_c$  superconductor by new critical state model with  $M_{eq}$ , *Physica C* **353**, 111 (2001).
- [41] N. A. Nizhelskiy, O. L. Poluschenko, and V. A. Matveev, Employment of Gd-Ba-Cu-O elongated seeds in top-seeded melt-growth processing of Y-Ba-Cu-O superconductors, *Supercond. Sci. Technol.* **20**, 81 (2007).
- [42] R. Liang, D. A. Bonn, and W. N. Hardy, Evaluation of  $\text{CuO}_2$  plane hole doping in  $\text{YBa}_2\text{Cu}_3\text{O}_{6+x}$  single crystals, *Phys. Rev. B* **73**, 180505(R) (2006).
- [43] F. Gömöry, Characterization of high-temperature superconductors by ac susceptibility measurements, *Supercond. Sci. Technol.* **10**, 523 (1997).
- [44] K. S. Pigalskiy, Enhancement of the intrinsic pinning by a magnetic field in a single crystal of high-temperature superconductor  $\text{TmBa}_2\text{Cu}_3\text{O}_y$ , *Phys. Solid State* **59**, 450 (2017).
- [45] W. N. Hardy, D. A. Bonn, D. C. Morgan, R. Liang, and K. Zhang, Precision Measurements of the Temperature Dependence of  $\lambda$  in  $\text{YBa}_2\text{Cu}_3\text{O}_{6.95}$ : Strong Evidence for Nodes in the Gap Function, *Phys. Rev. Lett.* **70**, 3999 (1993).
- [46] L. P. Gor'kov, Microscopic derivation of the Ginzburg-Landau equations in the theory of superconductivity, *Sov. Phys. JETP* **9**, 1364 (1959).
- [47] L. G. Mamsurova, K. S. Pigalskiy, N. G. Trusevich, A. A. Vishnev, M. A. Rogova, S. Yu. Gavrilkin, and A. Yu. Tsvetkov, Enhancement of pseudogap anomalies induced by nanoscale structural inhomogeneity in  $\text{YBa}_2\text{Cu}_3\text{O}_{6.93}$  high- $T_c$  superconductor, *JETP Lett.* **102**, 662 (2015).
- [48] A. A. Zhukov, E. T. Filby, P. A. J. de Groot, H. Küpfer, and T. Wolf, Vortex phases in  $\text{YBa}_2\text{Cu}_3\text{O}_y$  for B||CuO: impact of regular and random pinning, *Physica C* **408–410**, 541 (2004).
- [49] Y. B. Kim, C. F. Hempstead, and A. R. Strnad, Magnetization and critical supercurrents, *Phys. Rev.* **129**, 528 (1963).
- [50] P. W. Anderson, Theory of Flux Creep in Hard Superconductors, *Phys. Rev. Lett.* **9**, 309 (1962).
- [51] M. D. Ainslie and H. Fujishiro, Modeling of bulk superconductor magnetization, *Supercond. Sci. Technol.* **28**, 053002 (2015).
- [52] V. V. Bryksin and S. N. Dorogovtsev, Critical state of a nonuniform Josephson junction, *Sov. Phys. JETP* **75**, 558 (1992).
- [53] S. E. Savel'ev and V. S. Gorbachev, Microscopic critical-state model for a hard superconductor, *JETP* **83**, 570 (1996).